Journal of Catalysis 287 (2012) 124–137

Contents lists available at SciVerse ScienceDirect

Journal of Catalysis

journal homepage: www.elsevier.com/locate/jcat

Understanding the stability of Co-supported catalysts during ethanol reforming as addressed by *in situ* temperature and spatial resolved XAFS analysis

C.N. Ávila-Neto [a], J.W.C. Liberatori [a], A.M. da Silva [b], D. Zanchet [c], C.E. Hori [d], F.B. Noronha [b], J.M.C. Bueno [a,*]

[a] Departamento de Engenharia Química, Universidade Federal de São Carlos, C.P. 676, 13565-905 São Carlos, SP, Brazil
[b] Instituto Nacional de Tecnologia (INT), Av. Venezuela 82, CEP 20081-312, Rio de Janeiro, Brazil
[c] Instituto de Química, Universidade Estadual de Campinas (UNICAMP), C.P. 6154, 13083-970 Campinas, SP, Brazil
[d] Faculdade de Engenharia Química, Universidade Federal de Uberlândia, Av. João Naves de Ávila 2121, Campus Santa Monica – Bloco 1K, 38400-902 Uberlândia, MG, Brazil

ARTICLE INFO

Article history:
Received 4 August 2011
Revised 7 November 2011
Accepted 15 December 2011
Available online 9 January 2012

Keywords:
Hydrogen production
Ethanol reforming
CeO_2
Co-supported catalysts
In situ XAFS

ABSTRACT

Co catalysts, based on alumina supports modified with La_2O_3 and CeO_2, have been explored in the steam reforming of ethanol (SRE). The addition of oxygen in the reactants, process called oxy-reforming of ethanol (ORE), and the effect of adding Pt as a promoter were also addressed. One of the main challenges of this system is to hinder carbon deposition that leads to catalyst deactivation. In this work, the stability against carbon deposition was correlated to the control of the Co^{2+}/Co^0 ratio, which was addressed by *in situ* temperature-resolved X-ray absorption near edge spectroscopy (XANES). Temperature- and spatial resolved XANES indicated that the nature of supports, the presence/absence of Pt promoter and the composition of oxidants (water and oxygen) in the feed stream determine the degree of reduction of Co under reaction conditions. The control of the Co^{2+}/Co^0 ratio can equilibrate the steps of ethanol activation and carbon oxidation, resulting in stable catalysts.

1. Introduction

Hydrogen is an important feedstock for fertilizer production and has a crucial role in petroleum refining to reduce impact of fuels on the environment. In the near future, it is expected that hydrogen will become an important energy carrier for use in fuel cells. The production of hydrogen from renewable sources such as ethanol has received special attention due to the environment appeal of this route. Hydrogen can be produced by steam reforming of ethanol (SRE) (Eq. (1)) and steam reforming of ethanol with addition of oxygen in reactants, called oxy-reforming of ethanol (ORE), both reactions catalyzed by metal surfaces.

$$C_2H_5OH + H_2O \rightarrow 2CO_2 + 4H_2 \quad (1)$$

Density functional theory (DFT) studies on decomposition of ethanol over Pt(1 1 1) surfaces suggest that the abstraction of H from ethanol leads to the formation of intermediate OC–CH_x and subsequent cleavage of C–C bond yielding CO and CH_x species [1,2]. These calculations are in agreement with experimental data obtained for SRE on Co- and Ni-supported catalysts [3,4]. The experimental data indicate that the hydrogenation of CH_x species to CH_4 is favored at low temperatures [3,4]. The formation of CH_4, undesirable for maximizing the H_2 production, can be avoided using transition metals with high reactivity to CH_x species and low H hindrance, favoring the decomposition of CH_x species to C and H_2 via a pyrolytic mechanism [5]. On the other hand, this high reactivity of the metal implies in high activity for C–C bond cleavage and consequently C accumulates on metal surface. In this case, the presence of O species is crucial to reestablish the accessibility to these sites by C oxidation. The use of metals with low occupancy of the *d* orbital can contribute to both strong O interaction and high activity for C–C bond cleavage. However, if not kinetically equilibrated, these properties can result in deactivation due to the blockage of active sites by carbon deposits or due to the oxidation of active sites. Among the metals with low occupancy of the *d* orbital, Co [4,6] and Rh [7,8] have been described as active for reforming of ethanol.

The performance of catalysts is strongly influenced by the nature of support, which adsorbs ethanol and may lead to undesirable by-products. One critical case is the presence of acidic surfaces, which favors the ethanol dehydration forming ethylene and other by-products from the condensation of acetaldehyde [3,9,10]. The relative reaction rates on the support and on the metal directly influence the distribution of products. Thus, metals with higher activity are desirable. On the other hand, the increase in activity results in an increase in C on catalyst surface. In this case, a cooperative effect of O transfer from oxides to the metal–support interface will be desirable to promote oxidation of C and obtain active and stable catalysts. Considering that Co (i) has a high activity for the cleavage of C–H and C–C bonds and (ii) enables a higher free energy of adsorbed O species relative to other transition metals [5], these properties may confer

* Corresponding author. Fax: +55 16 33518266.
E-mail address: jmcb@ufscar.br (J.M.C. Bueno).

0021-9517/$ - see front matter © 2011 Elsevier Inc. All rights reserved.
doi:10.1016/j.jcat.2011.12.013

potential active sites for obtaining kinetically equilibrated catalysts for reforming of ethanol.

Recently, attention has been attracted to hydrogen production from different reaction, such as SRE and ORE, using Co-based catalysts supported on various oxides, such as Al_2O_3, MgO, ZnO, SiO_2, ZrO_2, CeO_2 and CeO_2–ZrO_2 [11–20]. In spite of reportedly high activities and selectivities, Co-based catalysts still undergo significant deactivation, which is generally attributed to Co particle sintering, carbon deposition and oxidation of the metallic Co particles. Carbon deposition strongly depends on the reaction conditions, such as reaction temperature, water/ethanol molar ratio and oxygen/ethanol molar ratio. Oxygen addition to the feed enhances the gasification rate of the carbon deposits improving the catalyst stability. However, it may lead to oxidation of the metallic Co particles, which can result in activity loss in the reforming reactions [21–24]. For example, Co/SiO_2, Co–Rh/SiO_2 and Co–Ru/SiO_2 catalysts deactivated under ORE carried out between 623 and 673 K [25]. The decrease in ethanol conversion was accompanied by a decrease in hydrogen selectivity and an increase in acetaldehyde selectivity. The authors proposed that oxygen from the feed oxidized the surface of Co particles and the Co oxide favored the dehydrogenation of ethanol to acetaldehyde. The oxidation of Co particles was inhibited or decreased by the addition of a noble metal (e.g., Rh, Ru). The coexistence of metallic Co and CoO_x phases was also observed in CeO_2- and CeO_2–ZrO_2-supported Co catalysts [18,20,26–29]. It is clear that the dependence on the degree of reduction of Co with the composition of reactants in the feed stream and with the type of support should not be neglected, and it has to be balanced with these requirements to decreasing the carbon deposition. It is important to stress that the changes in the oxidation state of Co have not been investigated under *reaction* conditions by using techniques such as XANES. The characterization of the nature of the active sites *under reaction conditions* is still a challenge, which is becoming less elusive with time.

In this work, we examine the phase changes of Co in Pt-promoted and unpromoted Co catalysts supported on Al_2O_3, La_2O_3/Al_2O_3, CeO_2/Al_2O_3 and CeO_2/$MgAl_2O_4$ in SRE and ORE reactions. Special effort was done to perform *in situ* characterization by XANES as a function of temperature and reaction conditions. The strong spatial dependence of the oxidation state of Co along the reactor was also addressed. The experiments aimed to contribute to the elucidation of issues concerning the Co-catalyzed ethanol reforming reactions such as (i) the sensitivity of stability to the amount of oxygen in the feed stream, (ii) the importance of support nature on catalyst stability and (iii) possible reasons of deactivation.

2. Experimental

2.1. Catalyst preparation

Commercial γ-Al_2O_3 (Strem Chemicals, $S_{BET} = 200\ m^2\ g^{-1}$) or $MgAl_2O_4$ synthesized by sol–gel method was used as support. The commercial γ-Al_2O_3 was calcined at 773 K (10 K min^{-1}) during 3 h under flow of 30 mL min^{-1} of synthetic air in order to remove moisture and any impurities adsorbed.

2.1.1. Synthesis of sol–gel $MgAl_2O_4$

A solution containing 13 g of aluminum tri-*sec*-butylate (Merck, 97%) diluted in 96.6 mL of ethanol was added to a solution containing 6.8 g of magnesium nitrate hexahydrate (Sigma–Aldrich, ≥99%) diluted in 13.5 mL of water, keeping the molar ratio of $MgAl_2O_4$. After stirring and refluxing constantly at 343 K for 1 h, 7.5 mL of ammonium hydroxide was added to the mixture and kept under reflux for 14 h. The solution was dried at room temperature during 48 h followed by a second treatment at 383 K for 4 h. The powder was then crushed until there was no visible change in its size, followed by treatment under flow of 80 mL min^{-1} of synthetic air at 1073 K (5 K min^{-1}) for 4 h.

2.1.2. Synthesis of Ce-–Al_2O_3, Ce–$MgAl_2O_4$ and La–Al_2O_3 with 12 wt.% Ce or La

Supports containing 12 wt.% of Ce or La were synthesized by incipient wetness impregnation of γ-Al_2O_3 or $MgAl_2O_4$ using aqueous solutions of cerium ammonium nitrate (Degussa, 99.99%) or lanthanum nitrate hydrate (Aldrich, 99.9%), respectively. The impregnated solids were dried at 373 K for 12 h and calcined at 1173 K (10 K min^{-1}) for 12 h under a flow of 80 mL min^{-1} of synthetic air.

2.1.3. Impregnation of supports with 12 wt.% Co and 0.05 wt.% Pt

The γ-Al_2O_3, Ce–Al_2O_3, La–Al_2O_3 and Ce–$MgAl_2O_4$ supports were impregnated with aqueous solutions of Cobalt nitrate hexahydrate (Aldrich, 99%) to contain 12 wt.% Co, followed by drying (383 K for 12 h) and calcination at 723 K (10 K min^{-1} for 12 h) in synthetic air. The addition of Pt to the Co catalysts was done by incipient wetness with aqueous solutions of hexachloroplatinic acid hexahydrate (Umicore) to contain 0.05 wt.% Pt. The samples were dried (383 K for 12 h) and calcined at 723 K (10 K min^{-1} for 2 h) under flow of synthetic air. The Co-based samples were defined as Co/Al, Co/Ce–Al, Co/La–Al and Co/Ce–AM, while the Co-based catalysts promoted with Pt were defined as Pt–Co/Al, Pt–Co/Ce–Al and Pt–Co/La–Al (Al and AM stand for γ-Al_2O_3 and $MgAl_2O_4$, respectively).

2.2. Characterization

Temperature-programmed reductions (TPR) were performed on a Micromeritics Pulse Chemisorb 2705 operating at atmospheric pressure. Prior to reduction, the samples (150 mg) were treated at 473 K for 2 h under N_2 flow and cooled to room temperature. Following, the samples were heated up to 1273 K (10 K min^{-1}) under 30 mL min^{-1} of a 5 v% H_2/N_2 mixture. Hydrogen uptake was monitored by a thermal conductivity detector (TCD) previously calibrated with a CuO sample.

BET surface areas of the samples were measured by N_2 adsorption at 77 K using a Quantachrome Nova 1200.

X-ray diffraction (XRD) patterns were recorded on a Rigaku DMAX 2500 PC diffractometer employing Cu Kα radiation (λ = 1.54056 Å) with a Ni filter. The 2θ angle was swept from 20° to 80° with step size of 0.02° and counting time of 1 s. To estimate the crystallite mean diameter of the Co_3O_4 particles, the XRD pattern of each catalyst was subtracted from the XRD pattern of the corresponding support, and the Scherrer's equation was applied to (3 1 1) reflection.

Hydrogen chemisorption experiments were performed on a Quantachrome Autosorb-1C. Prior to adsorption, the samples were activated *in situ* under 50 mL min^{-1} H_2 flow following the steps: (i) 2 K min^{-1} up to 373 K (holding time 30 min), (ii) 2 K min^{-1} up to 473 K (holding time 60 min) and 10 K min^{-1} up to 973 K (holding time 120 min). The system was evacuated for 30 min at 923 K and cooled down at 5 K min^{-1}. The H_2 adsorption and desorption were performed as described in previous work [30]. The sample was cooled to room temperature in H_2 flow and exposed for 1 h to H_2 to ensure the maximum adsorption. Next, samples were cooled to −243 K and purged in Ar for 1 h. Hydrogen desorption was obtained by heating at 10 K min^{-1} at 30 mL min^{-1} Ar flow. The H_2 desorbed was monitored with a TCD.

FT-IR spectra of adsorbed CO in the 2200–1700 cm^{-1} region were recorded on a Thermo Nicolet NEXUS 4700 FT-IR Spectrometer equipped with a MCT detector and a diffuse reflectance infrared Fourier transform spectroscopy reaction cell with CaF_2 windows

(DRIFT HTHV cell – Spectra Tech). Prior to the analyses, the samples were reduced at 973 K (10 K min^{-1}) for 3 h under H_2 flow. The samples were cooled to room temperature, transferred to the DRIFTS cell and reduced *in situ* at 773 K under flow of a 25 v% H_2/N_2 mixture. FT-IR spectra of adsorbed CO were collected after injection of 0.5 mL of CO in the DRIFTS cell. Following, desorption spectra were collected after injection of N_2 with successive heating and cooling at different temperatures to obtain the spectra at room temperature.

Scanning electron microscopy (SEM) images were recorded on a Philips XL 30 SEM before and after catalysts were exposed to ORE and SRE reactions. The fresh and used catalysts were dispersed in acetone, and the suspension was dropped onto a stainless steel sample holder. Then, gold powder was evaporated on each sample to form a thin layer.

The samples were characterized by transmission electron microscopy (TEM) using a JEOL JEM 3010 microscope, operating at 300 kV (1.7 Å point resolution) at the Brazilian Synchrotron Light Laboratory (LNLS). The supported catalysts were dispersed in isopropyl alcohol and deposited on amorphous carbon-coated copper grids.

X-ray absorption near edge spectroscopy (XANES) was measured at the Co K-edge (7709 eV) *in situ* conditions at the D06A-DXAS beamline of the LNLS. The D06A-DXAS is a dispersive beamline equipped with a curved Si(1 1 1) monochromator operating in Bragg mode that selects radiation from a bending magnet source in the X-ray range from 4 keV up to 14 keV and focuses it at the sample position [31,32]. An exposure time of around 0.3 s was employed for each measured spectrum, but the final spectrum was obtained after 100 accumulations (frames), giving 30 s of total acquisition time. Conversion of data, from pixel to energy, was accomplished by comparing measurements in conventional mode, in non-dispersive beamlines, with those in dispersive mode from the reference of metallic Co.

For the XANES experiments, the catalysts were first crushed and sieved to particle sizes smaller than 20 μ. Two different setups were used: (i) a self-supported pellet (for temperature-resolved analyses) placed inside a tubular quartz reactor (20 mm inside diameter and 440 mm X-ray path length), equipped with kapton refrigerated windows transparent to the X-ray beam [33]; and (ii) a capillary reactor with 1.2 mm internal diameter (for spatial/temperature-resolved analyses) homogeneously filled with 1 mm of catalyst powder.

Temperature-resolved XANES spectra were collected at different temperatures and atmospheres. XANES-H_2 spectra were acquired during TPR at 10 K min^{-1} up to 1023 K under flow of 200 mL min^{-1} of a 5 v% H_2/He mixture (holding time 30 min). After *in situ* reduction, temperature-resolved XANES-ORE or XANES-SRE spectra were acquired during heating of the reduced samples (i) at 10 K min^{-1} up to 733 K (holding time 30 min) and (ii) at 10 K min^{-1} from 733 K up to 773 K (holding time 30 min). The experiments were conducted under 3.9 mL min^{-1} of ORE (H_2O/ethanol/O_2 molar ratio = 3:1:0.5) or SRE (H_2O/ethanol molar ratio = 3:1) mixture diluted in 133 mL min^{-1} of He.

In the spatial/temperature-resolved XANES experiments, the 1-mm catalyst bed was kept in place by two plugs of quartz wool, and the X-ray beam was positioned in the direction normal to the wall of the capillary reactor. XANES-H_2 spectra were measured at 10 K min^{-1} up to 1023 K (holding time 30 min) under flow of 10 mL min^{-1} of a 5 v% H_2/He mixture with the beam positioned 0.4 mm after the entrance of the bed (P_4). After *in situ* reduction, the beam was kept at the same position (P_4), and XANES-ORE spectra were recorded during heating of the capillary at 10 K min^{-1} up to 773 K (holding time 30 min) under 1.1 mL min^{-1} of the ORE mixture diluted in 3.7 mL min^{-1} of He. After cooling to room temperature, the flow of reactants was maintained, and a second heating/cooling cycle was carried out at position P_4. Finally, the beam was shifted to the entrance of the bed (P_0), and a third and last heating cycle was performed. After this last cycle, the temperature was maintained in steady state at 773 K, and spectra were measured at six equally spaced points of the catalytic bed (0.2 mm steps, horizontal beam size of about 0.05 mm).

Energy calibration and normalization of the XANES spectra were performed with the open source software ATHENA-IFEFFIT [34]. In addition, a linear combination analysis of each spectrum obtained during temperature-resolved XANES-H_2, XANES-SRE or XANES-ORE measurements was performed using Co^0, CoO, Co_3O_4 and Co_2AlO_4 as reference compounds. Fig. S1 shows the normalized XANES spectra of the reference compounds. The linear fit was performed in the range from 20 eV below the edge and 30 eV beyond the edge. Despite the limitations of the linear combination approach for this kind of complex system, the goal was to get insights about the evolution of the Co phase by comparing the results acquired under different reaction conditions.

2.3. Catalytic test

2.3.1. Activity measurements

Activity measurements in SRE were carried out in a fixed bed quartz reactor (8 mm inside diameter and 230 mm length) operating isothermally at atmospheric pressure. Prior to the reaction, the catalyst bed (120 mg) was reduced *in situ* at 973 K (10 K min^{-1}) for 1 h under 50 mL min^{-1} of H_2. The activity to SRE and selectivity to products were measured from 523 up to 898 K with steps of 50 K. The reactant mixture (H_2O/ethanol molar ratio = 6) was fed to the reactor with the aid of an injection pump (KD Scientific – Model 100) coupled to the reactor, with liquid flow rate of 2 mL h^{-1}, eluted in 30 mL min^{-1} of He. The reactor effluent was analyzed online by gas chromatography employing a Varian 3600 CX equipped with a thermal conductivity detector (TCD) and a 20% Carbowax® 20 M ON 80/100 Chromosorb column, as described previously [1].

The molar fraction of a species *i*, y_i, was calculated using Eq. (2), and the conversion of ethanol was estimated using Eq. (3).

$$y_i\ (\%) = \frac{F_i}{(\sum_{j=1}^{N} F_j)} \times 100 \tag{2}$$

$$X_{Ethanol}(\%) = \frac{\sum_{j=1}^{N-H_2} \alpha_j F_j - \alpha_{Ethanol} F_{Ethanol}}{\sum_{j=1}^{N-H_2} \alpha_j F_j} \times 100 \tag{3}$$

In Eqs. (2) and (3), F_i and F_j are the molar flow of species *i* and *j*, respectively, α_j is the carbon number of specie *j*, and *N* is the number of species in the reactor outlet stream. Specifically in this work, $N = 8$, referring to the following species: H_2, CO, CO_2, CH_4, C_2H_4, acetaldehyde, methanol and ethanol.

2.3.2. Stability tests

Stability tests were conducted for SRE and ORE in a fixed bed quartz reactor operating isothermally at atmospheric pressure. To avoid temperature gradients, the catalysts (10 or 20 mg) were diluted in silicon carbide (SiC/catalyst weight ratio = 3). Prior to the reaction, the catalysts were reduced *in situ* at 973 K (10 K min^{-1}) for 1 h under 30 mL min^{-1} of H_2. The residence time (RT) was calculated from $W/F_{eth.}$ ratio, where *W* is the weight of catalyst in mg and F_{eth} is the mass flow rate of ethanol in mg min^{-1}. The reaction mixture of SRE (H_2O/ethanol molar ratio = 3) was fed to the reactor in order to obtain a RT of 4.4 min for ethanol on a 20 mg sample, which represents 9.6 mL min^{-1} of reaction mixture eluted in 67 mL min^{-1} of He. The reactor was maintained at 773 K during 6 h. Concerning the ORE stability tests, the reaction mixture (H_2O/ethanol/O_2 molar ratio = 3:1:0.5) was fed to the reactor in order to obtain 4.4 and 2.2 min residence times for ethanol relative to 20 and 10 mg of sample, respectively. To obtain these residence

times, the feed was composed of 10.7 mL min^{-1} of reaction mixture eluted in 66 mL min^{-1} of He. The reactor was maintained at 773 K during 30 h. The reaction products were analyzed online by gas chromatography employing an Agilent 3000A micro-GC equipped with a molecular sieve and a CP-PoraPLOT U using thermal conductivity detectors. The molar fraction of species *i* and the conversion of ethanol in the reactor outlet stream were calculated using Eqs. (2) and (3), respectively.

TOF at 580 K was calculated from the specific reaction rate and using the Co dispersion determined by H_2 chemisorption (Table 1). The feed comprised of H_2O/ethanol with molar ratio of 6 with total liquid flow rate of 2 mL h^{-1} eluted in 30 mL min^{-1} of He. The fractional distance from equilibrium in these experiments varied from 0.72 to 0.99. Net turnover rates (TOF_n) were used to obtain forward turnover rate (TOF_f) of the dehydrogenation reaction of ethanol, which is the main reaction that takes place at low temperature, as previously described in [4].

3. Results

The supports Al, La–Al, Ce–Al and Ce–AM show surface areas (S_{BET}) of 78, 74, 77 and 95 $m^2\ g^{-1}$, respectively. The surface areas of the catalysts were similar to the ones measured for the supports except for Ce-containing catalysts, that is, Co/Ce–Al, Pt–Co/Ce–Al and Co/Ce–AM, which presented lower surface areas of 66, 65 and 85 $m^2\ g^{-1}$, respectively (Table 1).

Fig. 1 presents the XRD patterns obtained for supports and unreduced catalysts. The catalysts show XRD peaks at 2θ equals to 36.8° and 44.8° characteristic of (311) and (400) reflections of Co_3O_4 spinel, respectively [28]. The apparent average crystallite sizes of Co_3O_4 are presented in Table 1, calculated from Scherrer equation using the (311) reflection. Most precursors have apparent crystallite sizes of Co_3O_4 around 9 nm, except the Ce-containing samples, which show larger values around 19 nm. La-containing samples did not show any diffraction lines relative to lanthanum oxides. Ce-containing catalysts show characteristic lines of the CeO_2 fluorite structure, that is, 2θ = 28.5°, 33.3°, 47.5° and 56.4°, corresponding to (111), (200), (220) and (311) reflections [35]. The apparent average crystallite sizes of ceria particles were 17 nm. The diffraction lines characteristic of metallic Co were hardly observed in the reduced samples (not shown).

In order to elucidate the phase changes of Co as a function of reduction temperature, the spectra obtained during temperature-resolved XANES-H_2 of the catalysts are shown in Fig. 2. Fig. 2A and D (left) shows the evolution of temperature-resolved XANES-H_2 spectra taken at the Co K-edge (the absorption intensity increases from lighter to darker color), and Fig. 2E and H (right) presents the results obtained by fitting the spectra using a linear combination of the reference compounds. The reduction temperatures observed from XANES-H_2 spectra are in good agreement with the *ex situ* TPR experiments (shown in Fig. S2). As an example, Fig. S3 shows some representative spectra of the Co/Al sample and the corresponding linear fit. It is worth to mention that the $CoAl_2O_4$ standard did not improve the fits. For Co/Al and Pt–Co/Al samples, the spectra show initially an intense white line characteristic of Co_3O_4 species [36]. The spectra profile indicates the formation of CoO and subsequently Co^0 by heating, reflecting a two-step reduction process ($Co_3O_4 \rightarrow CoO \rightarrow Co^0$), as previously described by Jacobs et al. [37]. For the Co/Al sample, the reduction of Co_3O_4 to CoO is achieved at 610 K, and the reduction of CoO to Co^0 occurs around 830 K (Fig. 2A). Similarly to the results previously described by Jacobs and Davis [36] and Kwak et al. [38], the addition of 0.05 wt.% of Pt to the Co/Al sample decreases the reduction temperatures of Co_3O_4 and CoO to 520 and 700 K, respectively (Fig. 2B). At 900 K, the reduced Co/Al sample presents around 80% of Co^0 and 20% of CoO, while the promoted Pt–Co/Al catalyst is completely reduced. The lower reduction temperature of the Pt-promoted sample is attributed to changes in the H_2 activation mechanism. H_2 is activated on Pt^0 sites rather than in the Co_3O_4 vacancies, producing atomic H, which is transferred to Co_3O_4 and CoO surfaces by hydrogen spillover [39]. The La-containing sample (Fig. 2C) shows reduction temperatures similar to the ones observed for Co/Al, although in this catalyst Co_3O_4 is reduced at lower temperatures and the rate of reduction of CoO is smaller. Interestingly, 35% of Co^{2+} remains unreduced at 973 K for the Co/La–Al sample. The Ce-containing sample (Fig. 2D) shows reduction temperatures similar to the ones

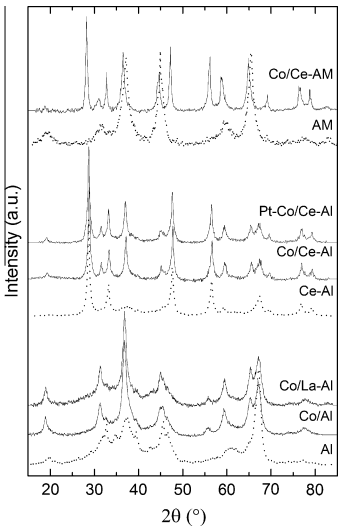

Fig. 1. XRD patterns of supports and unreduced catalysts.

Table 1
S_{BET} of Pt–Co/(La, Ce)–Al catalysts, D_{Co3O4} and D_{CeO2} obtained by XRD. H_2 uptake, TOF for dehydrogenation of ethanol and average rate deposition under SRE ($r_{carbon,SER}$) and ORE ($r_{carbon,ORE}$) reactions are also shown.

Sample	Co/Al	Co/La–Al	Co/Ce–Al	Pt–Co/Al	Pt–Co/La–Al	Pt–Co/Ce–Al
S_{BET} ($m^2\ g^{-1}$)	72	73	66	72	67	65
Particle size[ab](nm)	12	9	19 (17)	9	9	18 (15)
H_2 uptake (μmol g^{-1} cat)	36	39	29	42	–	53
TOF[c] (s^{-1})	0.07	–	0.12	0.1	–	–
$r_{carbon,SRE}$[d] ($mg_{carbon}\ g_{cat}^{-1}\ h^{-1}$)	24.9	34.1	16.5	39.1	78.4	61.6
$r_{carbon,ORE}$[d] ($mg_{carbon}\ g_{cat}^{-1}\ h^{-1}$)	1.7	2.1	0.1	2.5	3.3	0.3

[a] Values outside parenthesis are referred to Co_3O_4.
[b] Values between parenthesis are referred to CeO_2.
[c] TOF values calculated for dehydrogenation of ethanol at 580 K under steam reforming of ethanol (catalysts activated at 623 K and feed mixture of the 6:1 M ratio of H_2O/ethanol).
[d] Values between parenthesis are referred to stability test with 10 mg of catalysts, others are referred tests with 20 mg.

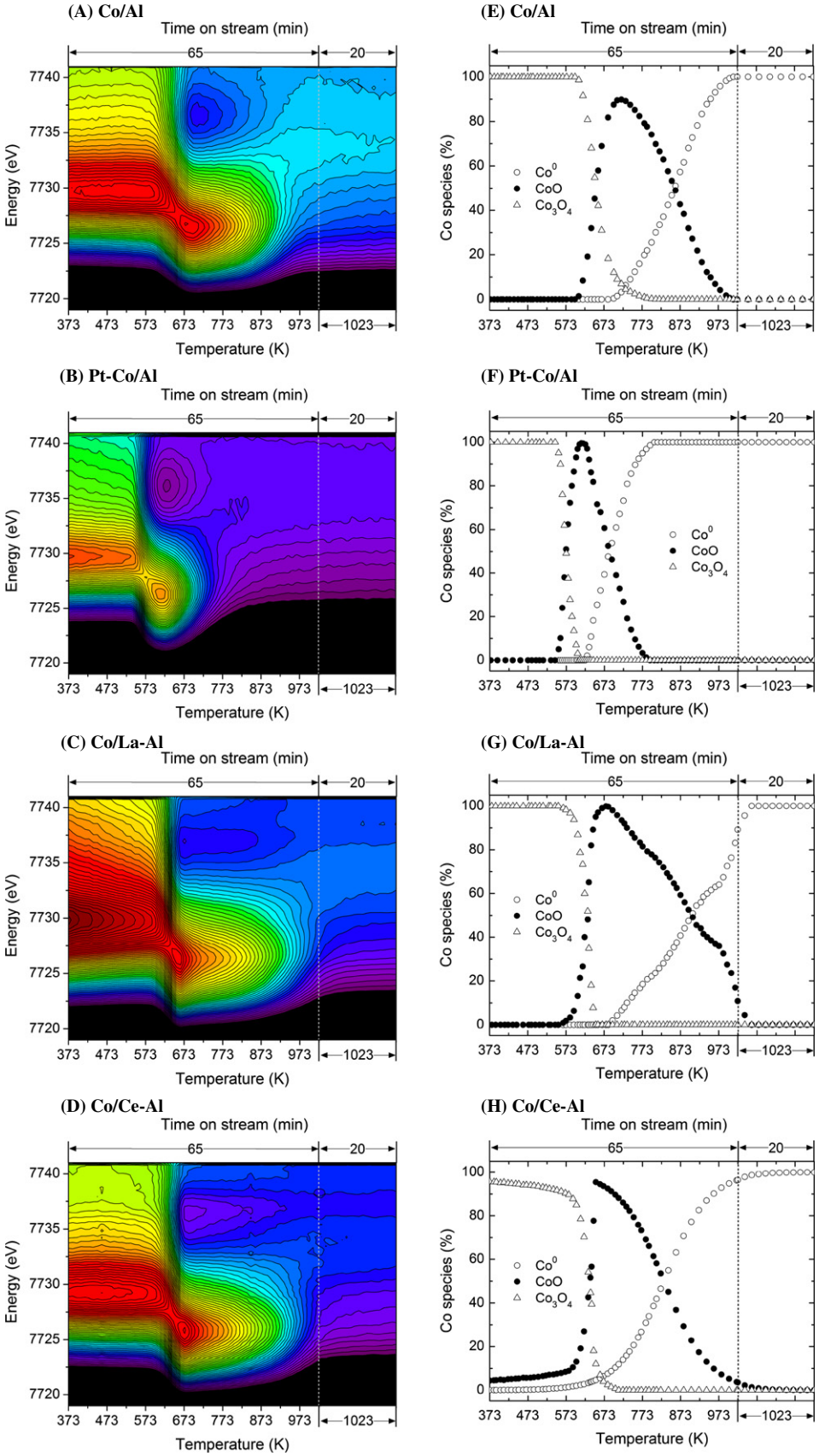

Fig. 2. Temperature-resolved XANES-H_2 spectra of Co/Al, Pt–Co/Al, Co/La–Al and Co/Ce–Al samples with respective percentage of Co species. Heating rate: 10 K min^{-1}; carrier flow: H_2/He (5/95). The absorption intensity increases from lighter to darker color. (For interpretation of the references to color in this figure legend, the reader is referred to the web version of this article.)

observed for Co/Al and Co/La–Al samples. The faster reduction of Co_3O_4 to CoO and higher maximum of CoO concentration for Co/La–Al and Co/Ce–Al reflect the lower interaction of Co_3O_4 with alumina when the surface has been modified by La or Ce. The addition of Pt to Co/La–Al and Co/Ce–Al (not shown) caused lower impact in the reduction temperatures than what was observed for Co/Al. Furthermore, the reductions of Co_3O_4 and CoO were facilitated by the presence of Pt, and CoO was fully reduced at 900 K.

FT-IR spectra of adsorbed CO on Co-supported catalysts at 298 K are presented in Fig. 3. Both sets of spectra, collect after CO Pulse (Fig. 3A) and after purge with N_2 (Fig. 3B), show bands at ca. 2170, 2060, 2020 and 1890 cm^{-1}. The band at 2170 cm^{-1} assigned to CO linearly adsorbed on Co^{2+} [40] is observed only for La-containing catalysts and with low intensity. The band at 2050–2095 cm^{-1}, typically assigned to CO linearly adsorbed on Pt^0 [41,42], could not be observed in these catalysts promoted with only 0.05 wt.% of Pt. The band at 1890 cm^{-1}, assigned to CO bonded in bridge form to two surface atoms of Co [43], is observed with low intensity for Co/Al and for Pt-promoted catalysts. The bands in the region 2050–2000 cm^{-1} are assigned to CO adsorbed in linear form on Co metal sites. The shoulder at 2040 cm^{-1} can be attributed to linear CO species adsorbed on metallic $Co^{\delta+}$ atoms perturbed by the support surface, while the band around 2010 cm^{-1} is attributed to CO linearly bonded to metallic Co [42]. The presence of La on Co/La–Al sample clearly suppresses the adsorption of CO, which may occur because of a dipole effect caused by geometric effect of LaO_x overlaying the Co particles. Ce-containing catalysts are very dark, and detection of CO was not possible. The addition of Pt over the Co/Al catalyst results in significant increase in metallic Co with higher electron density leading to a CO band at 2010 cm^{-1} (Fig. 3B).

Fig. 4 presents the ethanol conversion and selectivities as a function of temperature for SRE over Co/Al and Co/La–Al catalysts (H_2O/ethanol molar ratio = 6). All other catalysts behave similarly to Co/Al (Fig. 4 and S4). The distribution of products changes with increasing temperatures, and for Co/La–Al sample, ethanol decomposition is strongly suppressed at temperatures lower than 673 K. This is similar to what was observed by Liberatori et al. [3] for Ni/La–Al catalyst: ethanol dehydrogenates to acetaldehyde, which decomposes producing CH_4, CO and CO_2. The CH_4 curve shows two maximums around 673 and 823 K (Fig. S4). CO_2 is observed at temperatures higher than 640 K, and the $(CO + CO_2)/CH_4$ molar ratio is much larger than unity at temperatures above 673 K. As previously described in our work on Co nanoparticles supported on SiO_2 [2], this is a direct evidence that, at low temperature, there are two reaction pathways consuming the ethanol: (i) the decomposition of ethanol to CH_4, CO and H_2 and (ii) the reforming of ethanol to CO_2 and H_2. The water–gas shift (WGS) reaction (Eq. (4)) might contribute to the formation of CO_2 and H_2 at low temperature [44], which results in a maximum of CO and H_2 at temperatures higher than 773 K.

$$CO + H_2O \rightarrow CO_2 + H_2 \quad (4)$$

After reaching a maximum peak around 673 K, CO and CH_4 molar fractions decrease and CO_2 increases drastically, indicating that the rate of reforming of ethanol becomes faster than the rate of decomposition of ethanol to CO and CH_4. For the Co/La–Al sample at high temperatures, the fraction of CH_4 increases again, followed by decreasing of CO_2 and increasing of CO. This was clearly observed for Ce- and La-containing catalysts, which could indicate that CH_4 is formed mainly by hydrogenation of CO or CO_2. It has been reported that hydrogenation of CO to CH_4 is promoted with La and Ce in Co-based Al-supported catalysts [45] and Pd-based Ce-supported catalysts [46]. Interestingly, these results suggest that the ideal temperature to decrease CH_4 and increase H_2 molar fractions is comprised around 787 K. In this condition, the rate for hydrogenation of CO and CO_2 is lower, the reforming of ethanol is the main reaction, and the composition is closer to the equilibrium one for WGS. Finally, the decrease in CH_4 followed by the increase in H_2 and CO suggests that steam reforming of CH_4 occurs significantly at higher temperatures (823 K).

Fig. 5A presents the results of SRE for Co/Al catalyst as a function of time on stream (TOS) at 773 K and H_2O/ethanol molar ratio of 3. All catalysts in this study showed similar profiles of deactivation under SRE conditions. Characterization of the catalysts before and after SRE showed an intense formation of carbon filaments (Fig. 5B and C). The results of carbon deposition rates in SRE ($r_{carbon,SRE}$) (Table 1) suggest that the deactivation was indeed caused mainly by carbon deposition and formation of carbon filaments. The Co/Ce–Al catalyst showed the lowest $r_{carbon,SRE}$, but the rate was accentuated when the catalyst is promoted by Pt. Although the Al support is considered less efficient than La–Al or Ce–Al in supplying oxygen via CO_2 and H_2O to carbon oxidation, the $r_{carbon,SRE}$ on Co/Al is of the same order of magnitude to the ones verified for Co/La–Al and Co/Ce–Al catalysts. It seems that the nature of supports has no direct effect on $r_{carbon,SRE}$ at H_2O/ethanol molar ratio of 3. It is worth noting, however, that the effect of Ce on suppression of carbon deposition was previously observed at H_2O/ethanol molar ratio of 10 [6].

Interestingly, the $r_{carbon,SRE}$ follows a good linear fit with H_2 uptake for all catalysts (Fig. 6). Considering that all catalysts contain 12 wt.% of Co loading, the increase in H_2 uptake follows the same tendency decreasing of maximum reduction temperature of CoO (Fig. 2). Thus, these results suggest that the increase in H_2 uptake is mainly due the increased degree of reduction of CoO, which depend on nature of support and presence of Pt.

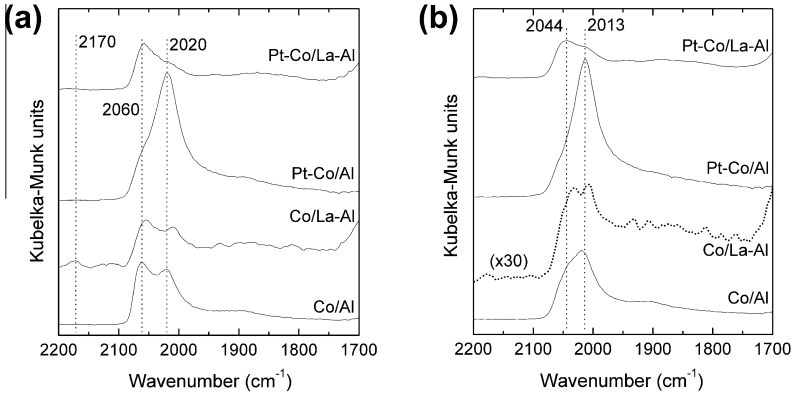

Fig. 3. FTIR-CO measurements of catalysts after H_2 activation at 973 K: (A) after CO Pulse and (B) after purge with N_2.

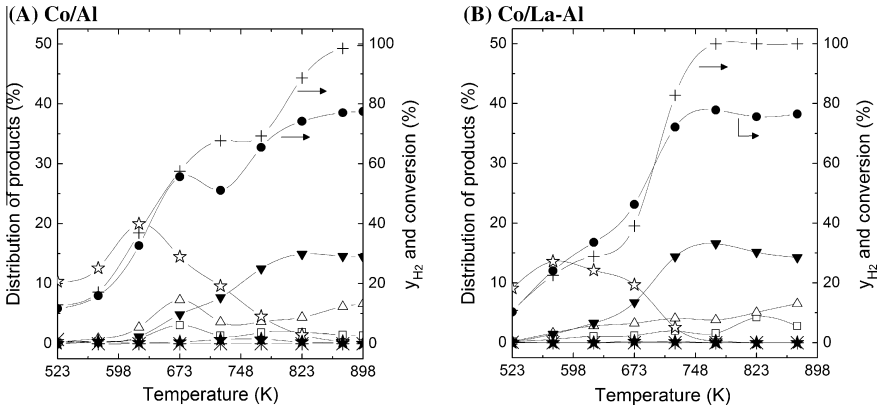

Fig. 4. Distribution of products for SRE (H_2O/ethanol = 6) as a function of TOS of (A) Co/Al and (B) Co/La–Al catalysts after H_2 activation at 773 K: (+) ethanol conversion, (●) H_2, (□) CH_4, (Δ) CO, (▼) CO_2, (★) ethylene and (☆) acetaldehyde.

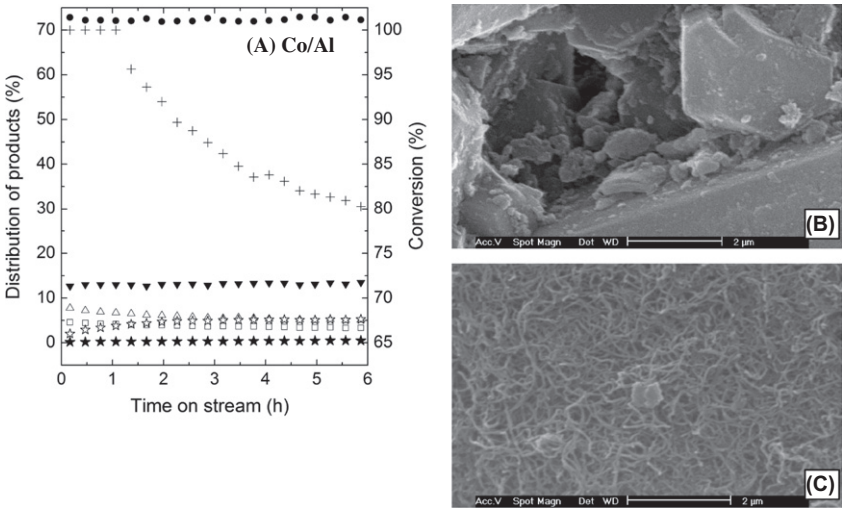

Fig. 5. Stability test under SRE conditions of Co/Al catalyst: (A) distribution of products as a function of TOS, (B) SEM image of fresh and (C) used catalyst. (T = 773 K, H_2O/ethanol = 3 and HRT = 4.4 min). (+) ethanol conversion, (●) H_2, (□) CH_4, (Δ) CO, (▼) CO_2, (★) ethylene and (☆) acetaldehyde.

Fig. 7 presents the distribution of products and ethanol conversion as a function of TOS when the La–Al and Ce–Al supports are exposed to ORE (H_2O/ethanol/O_2 = 3:1:0.5) at 773 K. The results show that the activity and distributions of products are strongly dependent on nature of support. For the La–Al support, the predominant product is acetaldehyde. On the other hand, for Ce–Al, the predominant products are acetaldehyde, CO and CO_2, while CH_4 and H_2 are formed at lower concentrations. Ethanol conversion is 100% for Ce–Al, whereas for La–Al, it reaches only 50%. Comparing these results, the Ce–Al support shows higher activity for the oxidation of ethanol to CO and CO_2, probably reflecting the oxygen storage capacity of ceria [47].

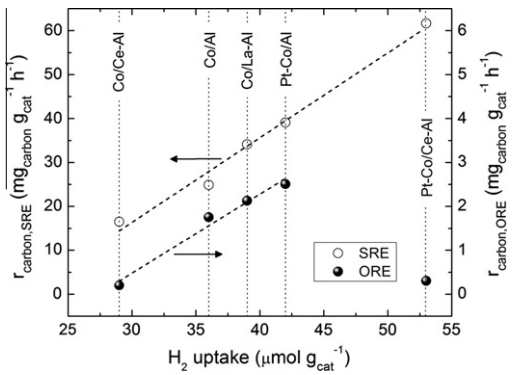

Fig. 6. Rate of carbon deposition versus H_2 uptake for (○) SRE and (●) ORE: experimental data and linear fit.

Fig. 8 presents the stability results when the catalysts (Co/Al, Co/La–Al and Co/Ce–Al) are exposed to reactant mixture of ORE at 773 K. The results were obtained using two different masses of catalyst, that is, 10 and 20 mg. Since the reactant mixture flow was kept constant, the use of distinct masses generated two residence times, which were called low residence time (LRT = 2.2 min) and high residence time (HRT = 4.4 min) for ethanol. Co/Al catalysts at LRT show a continuous deactivation and fast decrease on H_2 formation, while at HRT, the changes on total activity and formation of H_2 are less affected by TOS. At HRT, the selectivity to H_2 decreases in the order of Co/Al ≈ Co/La–Al > Co/Ce–Al, while the selectivity to CO_2 appears in the inverse order. The carbon deposition rates (Table 1) decrease in similar order to that observed for H_2 formation. It should be noted that the carbon deposition rate under ORE was much lower than under SRE (Table 1), and the carbon fibers are easily detected for all catalysts as shown in Fig. 9A and B, except for the Co/Ce–Al catalyst, where carbon fibers were not detected as shown in Fig. 9C and D. However, both rates follow a good linear fit with H_2 uptake (Fig. 6). These results clearly show that the nature of supports has no direct influence on

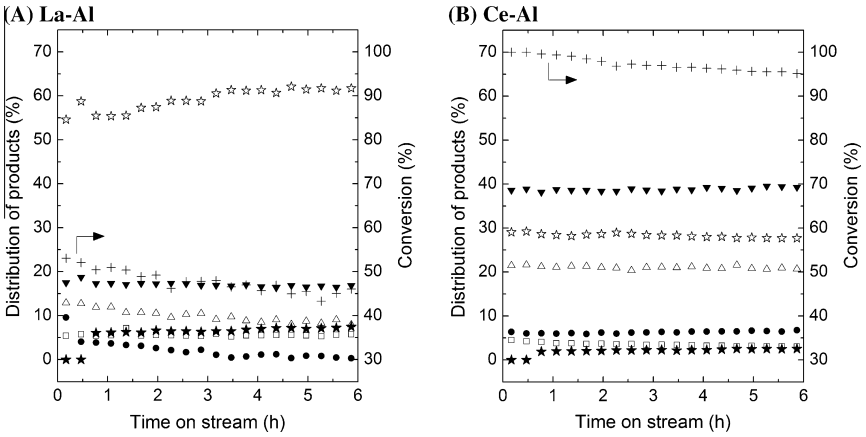

Fig. 7. Distribution of products for ORE on (A) La–Al and (B) Ce–Al supports as a function of TOS (T = 773 K, H_2O/ethanol/O_2 = 3:1:0.5 and HRT = 4.4 min): (+) ethanol conversion, (●) H_2, (□) CH_4, (Δ) CO, (▼) CO_2, (★) ethylene and (☆) acetaldehyde.

SRE and ORE reactions. The only exception is the Pt–Co/CeAl that in strong oxidizing conditions of ORE shows lower carbon deposition rates than with the one expected based on the H_2 uptake. Under the very oxidizing conditions of ORE, the oxidation of carbon on Co surface by O^* transferred from CeO_2 support becomes relevant.

Co/Al and Co/La–Al at LRT show a fast decrease in selectivity to H_2 within 2 h on stream, which is followed by an increase in selectivity to acetaldehyde. Co/Ce–Al at LRT shows a slow decrease in the selectivity to H_2. This deactivation occurs continuously during 30 h on stream, and at the same time, there is an increase in selectivity to acetaldehyde. Interestingly, Pt-promoted catalysts at LRT show a faster decrease on selectivity to H_2 (Fig. 10). For Pt–Co/Al catalyst, the formation of H_2 is suppressed after 25 h on stream with the increase in activity to oxidation of ethanol, reflecting the total oxidation of Co^0 to Co^{2+} sites. The higher deactivation rate to H_2 for Pt-promoted catalysts indicates that O_2 can be activated on Pt^0 sites, which transfer the atomic O to the Co^0 surface by oxygen spillover [48–50] and promote the oxidation of Co^0. This mechanism is analogous to the one that activates H_2 on Pt sites and promotes the reduction of Co oxides.

Comparing the catalytic results at LRT and HRT, there is a strong decrease in H_2 formation at LRT, whereas this effect is not as intense at HRT. These experiments show that the oxidation of Co sites occurs at the entrance of the catalytic bed, rich in oxygen, as evidenced by the catalytic result of Pt–Co/Al at LRT shown in Fig. 10A. Although the activity for H_2 production decreases sharply and is suppressed after 30 h of reaction at LRT, this decrease in activity is not as sharp at HRT (Fig. 10B). This fact suggests that with the total consumption of oxygen at the entrance of the bed, Co remains in the reduced form toward the end of the bed and H_2 is produced by the WGS reaction.

Fig. 9 presents SEM images of Co/Al, Co/La–Al and Co/Ce–Al catalysts used in ORE after 30 h on stream. The results confirmed the lower carbon deposition in ORE when compared to SRE reactions (Fig. 5), as already pointed out by the carbon deposition rates shown in Table 1. Carbon is hardly observed in Co/Ce–Al catalyst.

Fig. 11 presents the results of ethanol conversion and distribution of products for Co/Ce–AM under ORE at LRT conditions and 773 K. Different from the alumina-supported Co catalysts (Fig. 8 and 10), the Co/Ce–AM shows quite stable selectivities, mainly to H_2, suggesting that oxi-reduction characteristics of the active sites are maintained with TOS.

In order to get further information about the interaction of Co^{2+} with alumina under ORE conditions, the Co/CeAl sample was first reduced under H_2 at 650 K inside a capillary reactor. As demonstrated by temperature-resolved XANES-H_2 in Fig. 2D, this reduction temperature corresponds to the maximum reduction of Co_3O_4 to CoO. After this treatment, the sample was heated flowing He from 650 to 973 K. This last temperature corresponds to the temperature at which the samples were reduced prior to the stability tests in SRE and ORE conditions. After increasing the temperature under He flow, the Co/CeAl sample changed color from dark to blue. The XANES spectra of Co/CeAl sample after treatments and reference compounds are shown in Fig. 12. The spectra reveal that CoO reacted with the alumina support in the temperature at which the reaction is processed to form $CoAl_2O_4$ [51].

Fig. 13A provides information on the evolution of temperature-resolved XANES spectra under SRE (XANES-SRE) taken at the Co K-edge using a self-supported pellets placed inside a tubular quartz reactor. The corresponding fits using a linear combination of the standards Co_3O_4, CoO and Co^0 are shown in Fig. 13E. It is worth to mention that the inclusion of $CoAl_2O_4$ did not improve the fits for all samples under SRE or ORE (Fig. S5). Fig. 13B and C shows the evolution of temperature-resolved XANES spectra under ORE conditions (XANES-ORE) for Co/Ce–Al and Pt–Co/Ce–Al catalysts, respectively, and their corresponding linear fits are shown in Fig. 13F and G. Fig. 13D shows the distribution of products as a function of temperature obtained during XANES-ORE reaction on Pt–Co/Ce–Al catalyst.

Fig. 13H groups the profiles of oxidation states of Co as a function of temperature for Co/Ce–Al and Pt–Co/Ce–Al in SRE and ORE reactions. These profiles reflect the average oxidation state of Co in direction of the X-ray beam through the catalyst pellet. After reduction and exposition to reactants of SRE or ORE, all catalysts initially show an intense white line characteristic of oxidation of Co atoms corresponding to about 20–25% of Co^{2+} at 373 K. For SRE, all catalysts have profiles similar to the ones observed for Co/Ce–Al (Fig. 13A and E) and Co/Ce–AM (Fig. S6). Increasing the temperature under SRE conditions, the catalysts show an increase in degree of oxidation by H_2O. The maximum oxidation is about 50% of Co^{2+} found around 573 K. After this temperature, the fraction of reduced Co increases with temperature, and the point of maximum reduction is found at 733 K, reflecting the predominant reduction of catalysts by ethanol in this temperature region. Increasing the temperature under ORE conditions, in combination with mass spectrometry, the reforming products (H_2, CO and CO_2) are observed at temperatures higher than 623 K (Fig. 13G), while at lower temperatures, ethanol undergoes oxidative dehydrogenation. However, there are no rapid structural changes of Co (Fig. 12H).

For ORE reaction, all catalysts show a strong oxidation with increasing temperature, with maximum oxidation degree, around

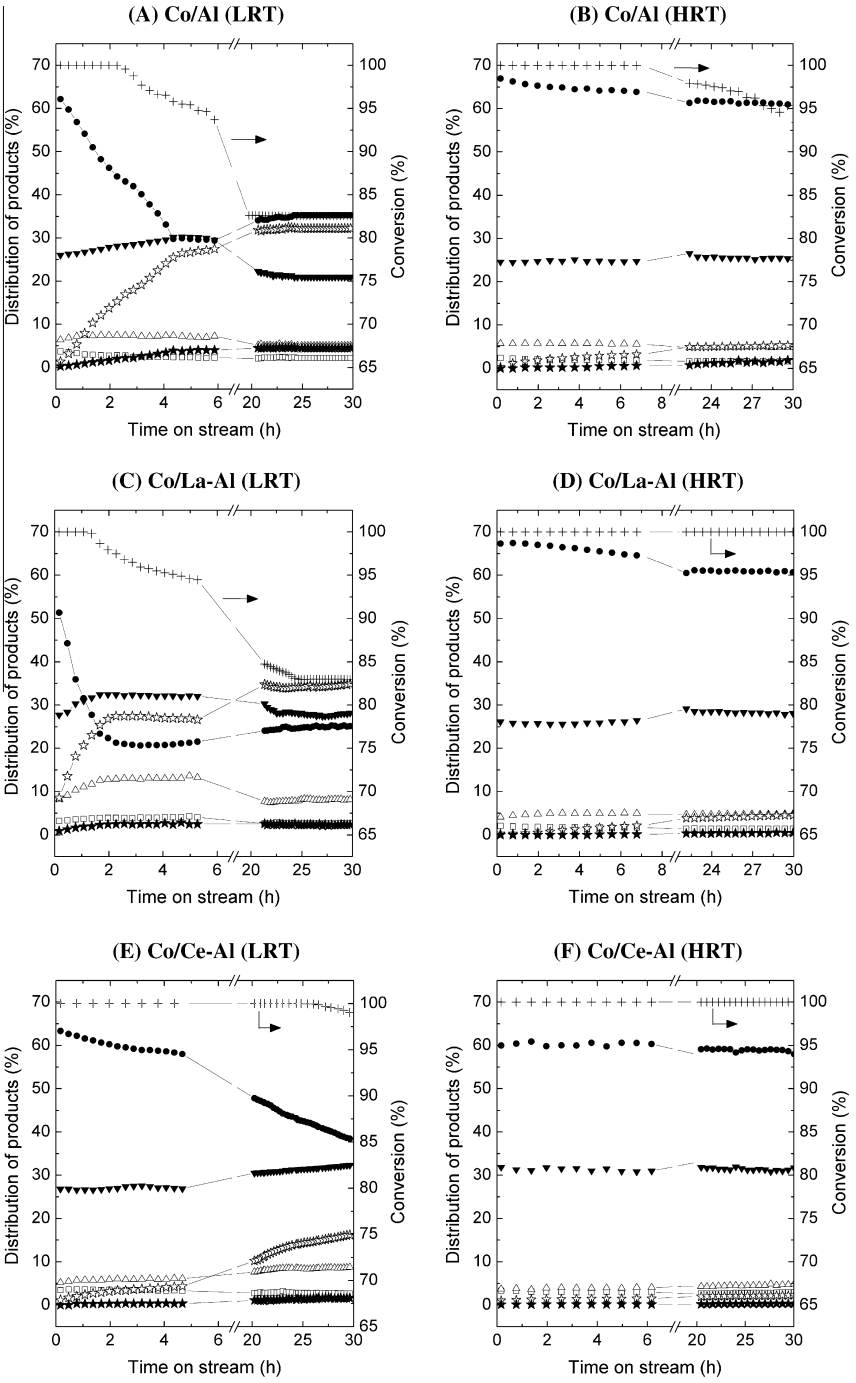

Fig. 8. Distribution of products for ORE on Co/Al, Co/La–Al and Co/Ce–Al catalysts as a function of TOS (T = 773 K and H_2O/ethanol/O_2 = 3:1:0.5): (+) ethanol conversion, (●) H_2, (□) CH_4, (Δ) CO, (▼) CO_2, (★) ethylene and (☆) acetaldehyde.

90%, at 673 K. The fraction of metallic Co increases with temperature, indicating that the oxidized region of the catalytic bed becomes thinner as the oxygen consumption becomes faster. When kept at 733 K, the reduction of Co^{2+} to Co^0 occurs slowly for all catalysts. The fraction of metallic Co also depends on the nature of support and on the presence of Pt, as shown in Fig. 13D and F. At 733 K, the degree of reduction increases in the following order: Co/Al < Co/Ce–Al < Pt–Co/Ce–Al. There are not simultaneous rapid structural changes or ignition during ORE, as observed during partial oxidation of methane over Pt-, Rh- and Pd-based catalysts [52,53]. In combination with mass spectrometry data, it was possible to observe that the oxidation degree of Co increases until 673 K. In the region where oxygen is totally consumed, the reduction of Co by ethanol becomes important, and products of reforming (H_2, Co and CO_2) are observed at 673 K. At this temperature, the ignition of ethanol reforming reaction occurs, while the catalysts structural changes are gradual with temperature, mainly by diffusion resistance in the catalyst pellets.

In order to minimize diffusion resistance effects and to obtain further information about the oxidation state of Co at different axial locations of the catalyst bed, a capillary reactor was employed and spatial and temperature-resolved XANES spectra for ORE reactions were measured for the Co/Ce–Al sample. The Co/Al catalyst presented a very fast growth of carbon filaments at the entrance

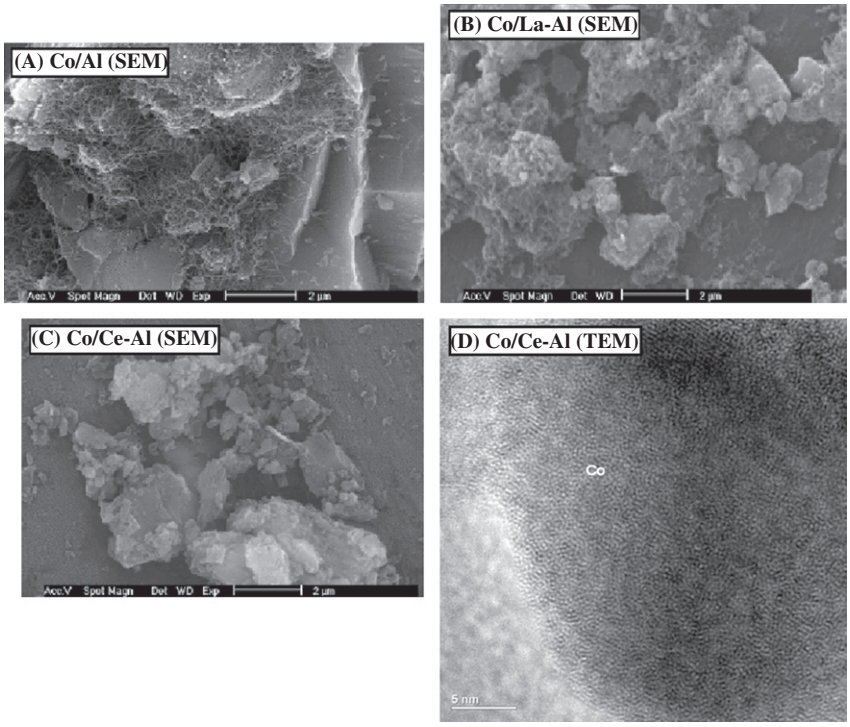

Fig. 9. SEM images of carbon filaments formed on (A) Co/Al and (B) Co/La–Al catalysts, and SEM image of Co/Ce–Al catalyst free of carbon filament (C) and (D) TEM image of Co/Ce–Al. All catalysts were exposed to ORE reaction (T = 773 K, H_2O/ethanol/O_2 = 3:1:0.5, HRT = 4.4 min and TOS = 30 h).

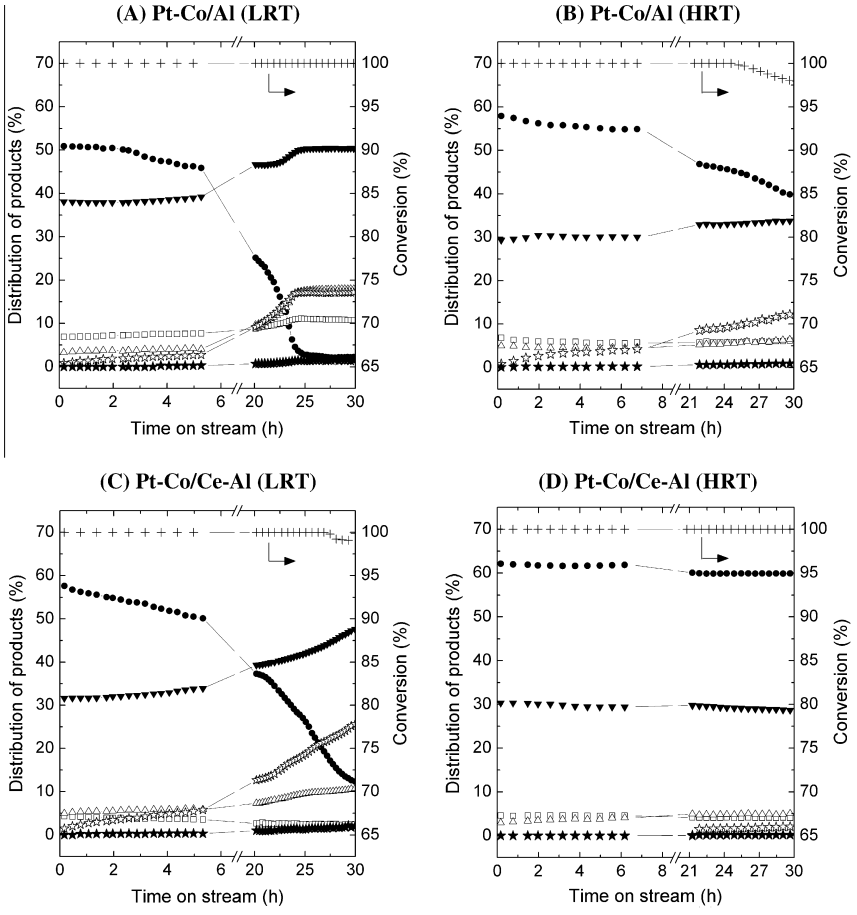

Fig. 10. Distribution of products for ORE on Pt–Co/Al and Pt–Co/Ce–Al catalysts as a function of TOS (T = 773 K and H_2O/ethanol/O_2 = 3:1:0.5): (+) ethanol conversion, (●) H_2, (□) CH_4, (Δ) CO, (▼) CO_2, (★) ethylene and (☆) acetaldehyde.

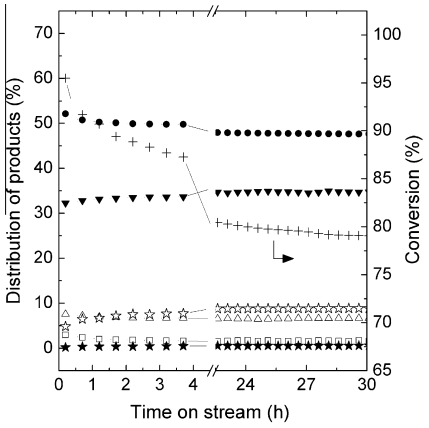

Fig. 11. Distribution of products for ORE of Co/Ce–AM catalyst as a function of TOS (T = 773 K and H_2O/ethanol/O_2 = 3:1:0.5). (+) ethanol conversion, (●) H_2, (□) CH_4, (Δ) CO, (▼) CO_2, (★) ethylene and (☆) acetaldehyde.

of the bed, which blocked the reactant flow soon after the temperature of 773 K was attained. Figs. 14 and S7 shows the evolution of Co oxidation states at three different axial regions of the bed as schematized. For the Co/Ce–Al sample, after *in situ* reduction, the X-ray beam was directed to the position 0.4 mm after the entrance of the bed (P_4), and the first heating cycle was performed under ORE atmosphere. The reactor was cooled to room temperature, the flow of reactants was maintained, and the second heating/cooling cycle was carried out at position P_4 with used sample. Following, the beam was shifted to the entrance of the bed (P_0), and the third and last heating cycle was performed in the same sample. As example of fits obtained, some spectra of ORE profiles for Co/Ce–Al sample in capillary reactor and their corresponding linear fitting from reference compounds are showed in Figs. S8 and S9. The $CoAl_2O_4$ improved the fits at entrance of the bed (P_0) (Fig. S8), demonstrating that $CoAl_2O_4$ is formed in thin layer at entrance of the bed.

The results indicate that at position P_4, in the first cycle of ORE and during heating, Co is re-oxidized, with maximum oxidation degree around 70–80%, at 700 K. At higher temperatures, Co^{2+} is promptly reduced, which indicates the ignition of the reforming reaction. After being cooled under ORE atmosphere, the catalyst appeared more oxidized than in the previous cycle, but the ignition of reforming occurred around 700 K, which is similar to what was observed in the first cycle. In the third heating cycle, at point P_0, unlike what was verified at position P_4, the catalyst remains predominantly oxidized due to the high concentration of oxygen and the presence of $CoAl_2O_4$ like species is observed.

Finishing the last heating cycle, the temperature was maintained at 773 K, and spectra were measured at six equally spaced points of the catalytic bed. The detailed profiles of Co^0 and CoO obtained by spatial resolved XANES spectra are shown in Fig. 15. The bed is predominantly oxidized at the first 0.3 mm, where the reduction front is situated. However, linear combination analysis suggests the presence of a significant percentage of $CoAl_2O_4$ at the entrance of bed. These facts imply that the reduction of the catalyst starts from the end region to the entrance, reflecting the concentration gradient of O_2 and H_2 over the catalyst bed.

4. Discussion

Alumina-supported Co_3O_4 precursor is reduced by a two-step process ($Co_3O_4 \rightarrow CoO \rightarrow Co^0$). The CoO species formed mainly during the first step of reduction shows high interaction with the alumina surface, resulting in Co/Al catalyst with low degree of reduction by activation at temperatures lower than 973 K. The addition of Ce or La on the Al_2O_3 surface decreases the interaction of the CoO species with the support. For Co/La–Al sample, a fraction of Co^{2+} species shows stronger interaction with La–Al support, being reduced at temperatures around 1023 K. The addition of Pt to Co/Al decreases the reduction temperatures of Co_3O_4 and CoO, resulting in more reducible catalysts. This lower temperature of reduction is attributed to H_2 activation on Pt^0 sites instead of vacancies in the Co oxides and transfer of atomic H to the Co_3O_4 and CoO surface by hydrogen spillover. The gain of reducibility associated with the decrease in interaction of the Co oxides and support added to the promotion effect of Pt is reflected in the increase in both H_2 uptake (Table 1) and CO adsorption band around 2010 cm^{-1}, characteristic of Co^0.

It has been demonstrated through experimental evidence that the rate of activation of ethanol occurs faster on metal surfaces

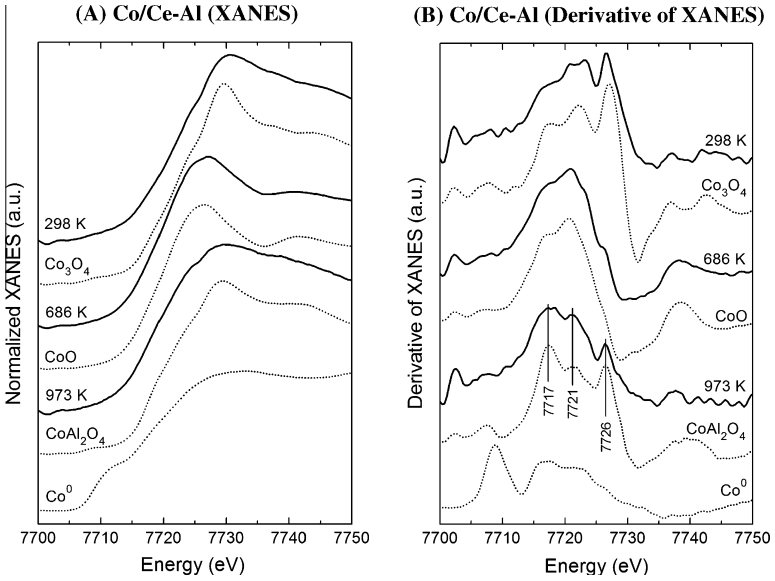

Fig. 12. (A) XANES spectra of standards (dot lines) and of Co/Ce–Al sample (solid lines) in capillary reactor, heating under H_2 up to 651 K, followed by heating under He up to 973 K. (B) Respective XANES derivative spectra.

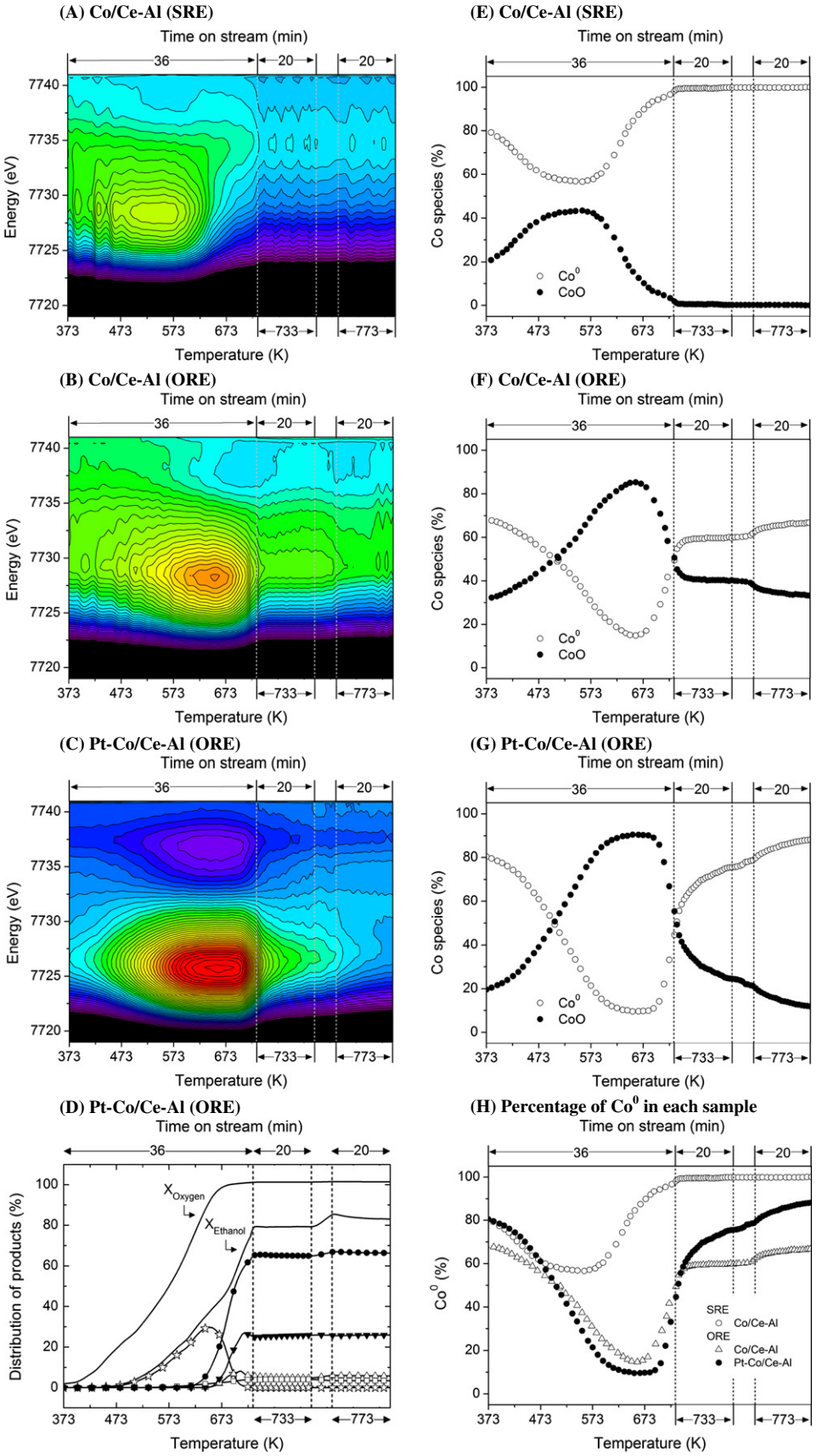

Fig. 13. (Left): Temperature-resolved XANES-SRE spectra of (A) Co/Ce–Al and XANES-ORE spectra of (C) Co/Ce–Al and (E) Pt–Co/Ce–Al catalysts, flowing reactants through of single catalyst pellet. The absorption intensity increases from lighter to darker color, and (G) composition of effluent of reactor in ORE and Pt–Co/Ce–Al. (Right): (B) distribution of products for SRE of Co/Ce–Al; (D) and (F) for ORE of Co/Ce–Al and Pt–Co/Ce–Al, respectively. (H) Groups the percentage of Co^0 calculated from XANES spectra. Samples reduced flowing H_2 at 973 K, cooled to 298 K and flow replaced by ORE mixture (H_2O/ethanol/O_2 = 3:1:0.5) or SRE mixture (H_2O/ethanol = 3). Heating rate: 10 K min^{-1}, flowing 133 mL min^{-1} of He and 3.9 mL min^{-1} of ORE mixture or 3.45 mL min^{-1} of SRE mixture. (For interpretation of the references to color in this figure legend, the reader is referred to the web version of this article.)

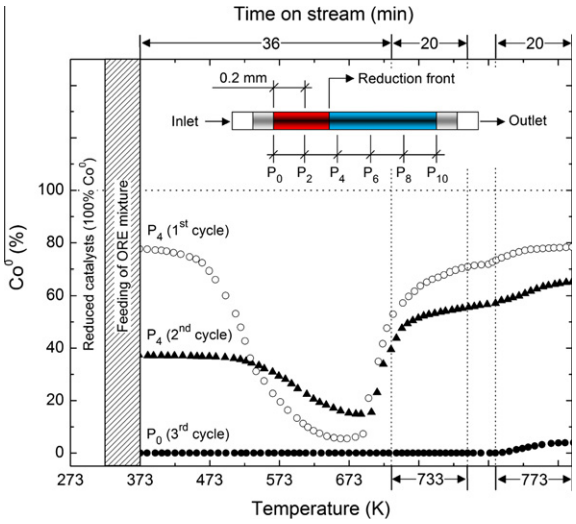

Fig. 14. Temperature-resolved XANES-ORE spectra of Co/Ce–Al catalyst flowing reactants through a capillary reactor: percentage of Co^0 calculated from XANES spectra. Sample reduced flowing H_2 at 973 K, cooled to 298 K and flow replaced by ORE mixture (H_2O/ethanol/O_2 = 3:1:0.5). Heating at 10 K min^{-1}, flowing 1.1 mL min^{-1} of ORE mixture diluted in 3.7 mL min^{-1} of He.

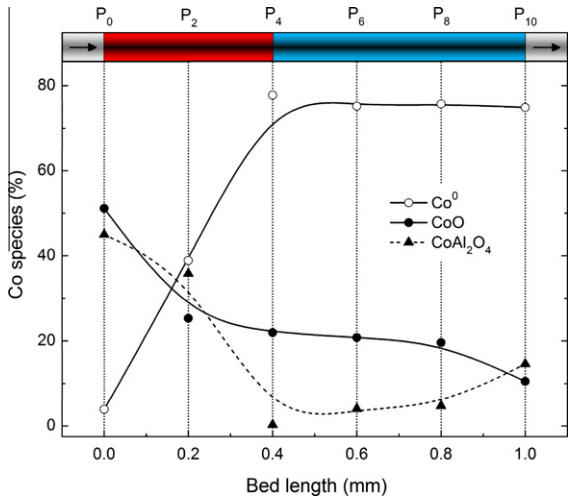

Fig. 15. Spatial resolved XANES-ORE spectra of Co/Ce–Al catalyst flowing ORE mixture (H_2O/ethanol/O_2 = 3:1:0.5) through capillary reactor at 973 K: percentage of Co^0, CoO and $CoAl_2O_4$ calculated from XANES spectra.

than in oxides [54]. Reforming occurs via an intermediate like OC–CH_x, with cleavage of C–C bond, decomposition of –CH_x species forming active C*, which can be removed by reaction with oxygen bound to the surface (O*) and formation of CO. Considering (i) the mechanism described, (ii) the fact that carbon accumulates on all Co catalysts under SRE conditions (H_2O/ethanol = 3) with formation of filaments and (iii) the linear correlation between carbon deposition rates for SRE and Co^0 sites, it is clear that the oxidation of C* is the kinetically-relevant step. Also, the steps of ethanol activation and C* oxidation can be equilibrated by decreasing the size of Co clusters. The support nature (Al, La–Al and Ce–Al) and the presence of Pt influence the size of Co clusters or the specific density of Co sites, but they do not influence the rates of C* oxidation, indicating that the activation of co-reactants H_2O or CO_2 on La–Al and Ce–Al is not relevant at low H_2O/ethanol ratio.

ORE reactions show high initial H_2 yield that decreased after only 5 h on stream at LRT experiments. For the Co/Ce–Al sample, which is free of carbon filaments after use in ORE (Fig. 9), this is associated with an increase in the yield of oxidation products (Fig. 8). XANES data acquired at the entrance of the catalytic bed demonstrate that Co is mainly oxidized in this region and that there is evidence of formation of $CoAl_2O_4$. This result suggests that the decrease in H_2 yield occurs mainly due to Co re-oxidation in Co/Ce–Al catalyst that is accelerated in by the promotion with Pt leading to total suppression of H_2 yield for Pt–Co/Al catalyst after 25 h on stream (Fig. 10). Considering that this effect occurs even when the catalyst is activated with reactant mixture, there are no obvious reasons for Co to re-oxidize continuously under operating conditions. Temperature-resolved XANES spectra under ORE conditions indicate that the presence of Pt promotes both the oxidation of Co by O_2 at low temperatures and the reduction of CoO at high temperatures. Therefore, Pt promotes the activation of O_2 transferring atomic O to the Co^0 surface by oxygen spillover [48–50]. Temperature-resolved XANES-H_2 and XANES-ORE spectra indicate that an analog mechanism occurs in the presence of H_2, that is, H_2 is activated on Pt sites, transferring atomic H by hydrogen spillover [39] to the CoO surface favoring reduction. Co^{2+} and Co^0 species coexist at a microdomain mainly at the oxidized zone at the entrance of the catalytic bed. It is likely that Co^{2+} ions diffuse into the support and occupy the vacant sites in tetrahedral positions of Al_2O_3 resulting in the loss of active of the Co sites at the entrance of the bed ($Co^0 \leftrightarrow CoO \rightarrow CoAl_2O_4$). A deactivation wave is propagated from the entrance of bed through all later regions containing O_2, and this effect is accelerated in Pt-promoted catalysts due to the increase in Co^{2+} species content. This hypothesis is supported by XANES results (Fig. 12) and the change of color when heating a CoO/Al_2O_3 sample in He at 973 K from dark to blue, which is an evidence of $CoAl_2O_4$ formation. Besides, using the aluminates such as $MgAl_2O_4$ (Co/Ce–AM) avoids the diffusion of Co^{2+} ions, and the yield of H_2 keeps its initial value at LRT, although the initial decreasing of ethanol conversion occurred in Co/Ce–AM catalyst (Fig. 11), indicating that the Co in pre-reduced catalyst is partially re-oxidized in contact with ORE reactants. Different than observed for Co supported on alumina, which occurs in the reaction of CoO with Al_2O_3, for Co/Ce–AM catalyst, the initial oxidation of Co is not enough to cause a decrease in H_2 yield at LRT.

The addition of oxygen to the reactants suppresses strongly the carbon deposition rate in ORE relative to SRE reactions, which is followed by significant increases in the Co^{2+}/Co ratio. The increase in H_2 uptakes resulted in catalysts with lower average Co^{2+}/Co ratios in ORE reactions and higher carbon deposition rates. However, we can infer that the properties of oxidation and reduction of Co in ORE mixture are determinant to carbon deposition rate. Concerning the thermodynamic analysis on simultaneous oxidation and re-reduction of small metallic Co crystallites, the standard free energy of formation of $Co + ½O_2 \leftrightarrow CoO$ and $CoO + H_2 \leftrightarrow Co + H_2O$ should depend on morphology of the crystallite [55] and on the metal-cluster curvature [56], in which oxidation of the metal is favored with decreasing both the metal particle sizes and the temperature [57]. This might be indicative that, under reaction conditions, the Co^{2+}/Co ratio should be controlled by manipulating composition of reactants and temperature, as well as by manipulating the Co cluster sizes. The Co^{2+}/Co^0 ratio is indirectly dependent on the nature of support, where the interaction of cobalt oxide with support determines the Co particles size and becomes more oxidized with the presence of Ce. Considering the spatial resolved XANES data that indicate that Co is mainly in oxidizing state at the entrance of the catalytic bed, Co^{2+} and Co^0 coexist, and Co^{2+}/Co^0 ratio decreases slowly throughout the bed at reaction temperature (773 K). Thus, it is reasonable to suppose that this creates the potential Co^0/CoO sites for oxidation of adsorbed C*. Hence, stable catalysts are found when the steps of activation of ethanol and oxidation of C* are equilibrated.

5. Conclusions

Under SRE at low H_2O/ethanol molar ratio (H_2O/ethanol = 3) on alumina-supported Co catalysts, the deactivation of catalysts occurs mainly by carbon deposition. The rate of carbon deposition is connected to the density of Co^0 sites, characterized by changes of H_2 uptake. The supports influence the degrees of reduction of Co and have indirect influence on the control of carbon deposition.

Deposition of carbon decreases with addition of O_2 in reactants in ORE. There are not simultaneous rapid structural changes, and ignition of ORE and Co^0 and Co^{2+} coexists at a microdomain at the oxidized zone in the entrance of the catalytic bed. The Co^{2+} ions diffuse in the support resulting in loss of active Co sites at the entrance of the bed ($Co^0 \leftrightarrow CoO \rightarrow CoAl_2O_4$). A deactivation wave is propagated from the entrance of bed through all later regions containing O_2, which is blocked when Co is supported on aluminates. The nature of supports and the presence of Pt promoter determine the degree of reduction of Co under reaction. The Co^{2+}/Co^0 ratio is strongly sensitive to the degree of Co reduction obtained in activation of catalysts, to the composition of oxidants reactants (O_2, H_2O) in the feed stream and temperature of reaction.

The CoCoO sites on surface, created by the presence of O_2, can control the rate of activation of ethanol and promote the oxidation of C^*. The control of the Co^{2+}/Co^0 ratio by manipulating the interaction of Co oxides with the support and by the composition of reactants can equilibrate the steps of ethanol activation and carbon oxidation, resulting in stable catalysts.

Acknowledgments

The authors gratefully acknowledge financial support from VALE and FAPESP (Fundação para o Amparo a Pesquisa do Estado de São Paulo-Brazil), FINEP (Financiadora de Estudos e Projetos) and the Brazilian Synchrotron Light Laboratory (LNLS), which is acknowledged for the use of its facilities and technical support in TEM (LME) and XAFS (DXAS and XAFS2 beamline) experiments.

Appendix A. Supplementary material

Supplementary data associated with this article can be found, in the online version, at doi:10.1016/j.jcat.2011.12.013.

References

[1] R. Alcalá, M. Mavrikakis, J.A. Dumesic, J. Catal. 218 (2003) 178–190.
[2] P. Ferrin, D. Simonetti, S. Kandoi, E. Kunkes, J.A. Dumesic, J.K. Nørskov, M. Mavrikakis, J. Am. Chem. Soc. 131 (2009) 5809–5815.
[3] J.W.C. Liberatori, R.U. Ribeiro, D. Zanchet, F.B. Noronha, J.M.C. Bueno, Appl. Catal. A 327 (2007) 197–204.
[4] R.U. Ribeiro, J.W.C. Liberatori, H. Winnishofer, J.M.C. Bueno, D. Zanchet, Appl. Catal. B 91 (2009) 670–678.
[5] G. Jones, J.G. Jakobsen, S.S. Shim, J. Kleis, M.P. Andersson, J. Rossmeisl, F. Abild-Pedersen, T. Bligaard, S. Helveg, B. Hinnemann, J.R. Rostrup-Nielsen, I. Chorkendorff, J. Sehested, J.K. Nørskov, J. Catal. 259 (2008) 147–160.
[6] H. Song, U.S. Ozkan, J. Catal. 261 (2009) 66–74.
[7] A. Birot, F. Epron, C. Descorme, D. Duprez, Appl. Catal. B 79 (2008) 17–25.
[8] A.M. da Silva, K.R. de Souza, G. Jacobs, U.M. Graham, B.H. Davis, L.V. Mattos, F.B. Noronha, Appl. Catal. B 102 (2011) 94–109.
[9] A. Machocki, A. Denis, W. Grzegorczyk, W. Gac, Appl. Surf. Sci. 256 (2010) 5551–5558.
[10] A.N. Fatsikostas, X.E. Verykios, J. Catal. 225 (2004) 439–452.
[11] F. Haga, T. Nakajima, H. Miya, S. Mishima, Catal. Lett. 48 (1997) 223–227.
[12] J. Llorca, N. Homs, J. Sales, P.R. de la Piscina, J. Catal. 209 (2002) 306–317.
[13] H. Song, L. Zhang, U.S. Ozkan, Green Chem. 9 (2007) 686–694.
[14] D.R. Sahoo, S. Vajpai, S. Patel, K.K. Pant, Chem. Eng. J. 125 (2007) 139–147.
[15] M.S. Batista, R.K.S. Santos, E.M. Assaf, J.M. Assaf, E.A. Ticianelli, J. Power Sources 134 (2004) 27–32.
[16] J.A. Anderson, M. Fernándes García, Supported metals in catalysis, in: G.J. Hutchings (Ed.), Catalytic Science Series, Imperial College Press, London, 2005, p. 380.
[17] S. Lin, D. Kim, S. Ha, Catal. Lett. 122 (2008) 295–301.
[18] S.S.Y. Lin, D.H. Kim, S.Y. Ha, Appl. Catal. A 355 (2009) 69–77.
[19] S.M. de Lima, A.M. da Silva, L.O.O. da Costa, U.M. Graham, G. Jacobs, B.H. Davis, L.V. Mattos, F.B. Noronha, J. Catal. 268 (2009) 268–281.
[20] S.S.Y. Lin, D.H. Kim, M.H. Engelhard, S.Y. Ha, J. Catal. 273 (2010) 229–235.
[21] F. Frusteri, S. Freni, V. Chiodo, S. Donato, G. Bonura, S. Cavallaro, Int. J. Hydrogen Energy 31 (2006) 2193–2199.
[22] J. Kugai, S. Velu, C. Song, M.H. Engelhard, Y. Chin, J. Catal. 238 (2006) 430–440.
[23] N. Laosiripojana, S. Assabumrungrat, Appl. Catal. A 327 (2007) 180–188.
[24] A.L.M. da Silva, L.V. Mattos, J.P. den Breejen, J.H. Bitter, K.P. de Jong, F.B. Noronha, Catal. Today 164 (2011) 262–267.
[25] E.B. Pereira, N. Homs, S. Marti, J.L.G. Fierro, P.R.J. de la Piscina, J. Catal. 257 (2008) 206–214.
[26] J. Llorca, J.-A. Dalmon, P. Ramírez de la Piscina, N. Homs, Appl. Catal. A 243 (2003) 261–269.
[27] J. Llorca, P. Ramírez de la Piscina, J.-A. Dalmon, N. Homs, Chem. Mater. 16 (2004) 3573–3578.
[28] V.A. de la Peña O'Shea, N. Homs, E.B. Pereira, R. Nafria, P. Ramírez de la Piscina, Catal. Today 126 (2007) 148–152.
[29] S. Tuti, F. Pepe, Catal. Lett. 122 (2008) 196–203.
[30] E.L. Rodrigues, J.M.C. Bueno, Appl. Catal. A: Gen. 232 (2002) 147–158 149.
[31] H.C.N. Tolentino, J.C. Cezar, N. Watanabe, C. Piamonteze, N.M. Souza-Neto, E. Tamura, A.Y. Ramos, R. Neueschwander, Phys. Scripta T115 (2005) 977–979.
[32] J.C. Cezar, N.M. Souza-Neto, C. Piamonteze, E. Tamura, F. Garcia, E.J. Carvalho, R.T. Neueschwander, A.Y. Ramos, H.C.N. Tolentino, A. Caneiro, N.E. Massa, M.J. Martinez-Lope, J.A. Alonso, J.-P. Itie, J. Synchr. Rad. 17 (2010) 93–102.
[33] C.T. Meneses, W.H. Flores, A.P. Sotero, E. Tamura, F. Garcia, J.M. Sasaki, J. Synchr. Rad. 13 (2006) 468–470.
[34] J. Mustre de Leon, J.J. Rehr, S.I. Zabinsky, R.C. Albers, Phys. Rev. B44 (1991) 4146.
[35] S.J. Duclos, Y.K. Vohra, A.L. Ruoff, A. Jayaraman, G.P. Espinosa, Phys. Rev., B 38 (1988) 7755.
[36] G. Jacobs, B.H. Davis, Appl. Catal. A 333 (2007) 192–201.
[37] G. Jacobs, J.A. Chaney, P.M. Patterson, T.K. Das, B.H. Davis, Appl. Catal. A 264 (2004) 203–212.
[38] C. Kwak, T.J. Park, D.J. Suh, Appl. Catal. A 278 (2005) 181–186.
[39] E. Baumgarten, E. Denecke, J. Catal. 95 (1985) 296–299.
[40] G. Kadinov, Ch. Bonev, S. Todorova, A. Palazov, J. Chem. Soc., Faraday Trans. 94 (1998) 3027.
[41] P.J.S. Prieto, A.P. Ferreira, P.S. Haddad, D. Zanchet, J.M.C. Bueno, J. Catal. 276 (2010) 351–359.
[42] J. Xu, J.T. Yates Jr., Surf. Sci. 327 (1995) 193–201.
[43] E.L. Rodrigues, J.M.C. Bueno, Appl. Catal. A 257 (2004) 201–211.
[44] R. Knapp, S.A. Wyrzgol, A. Jentys, J.A. Lercher, J. Catal. 276 (2010) 280–291.
[45] J. Barrault, A. Chafik, P. Gallezot, Appl. Catal. 67 (1990) 257–268.
[46] W.-J. Shen, Y. Ichihashi, H. Ando, Y. Matsumura, M. Okumura, M. Haruta, Appl. Catal. A 217 (2001) 231–239.
[47] A.M. da Silva, K.R. de Souza, L.V. Mattos, G. Jacobs, B.H. Davis, F.B. Noronha, Catal. Today 164 (2011) 234–239.
[48] A. Katsaounis, Z. Nikopoulou, X.E. Verykios, C.G. Vayenas, J. Catal. 222 (2004) 192–206.
[49] T. Inui, Y. Ono, Y. Takagi, Jin-Bae Kim, Appl. Catal. A: Gen. 202 (2000) 215–222.
[50] W. Curtis Conner Jr., J. John, L. Falconer, Chem. Rev. 95 (1995) 708–759.
[51] A. Moen, D.G. Nicholson, B.S. Clausen, P.L. Hansen, A. Molenbroek, G. Steffensen, Chem. Mater. 9 (1997) 1241–1247.
[52] B. Kimmerle, J.-D. Grunwaldt, A. Baiker, P. Glatzel, P. Boye, S. Stephan, C.G. Schroer, J. Phys. Chem. C 113 (2009) 3037–3040.
[53] Jan-Dierk Grunwaldt, M. Beier, B. Kimmerle, A. Baiker, M. Nachtegaal, B. Griesebock, D. Lützenkirchen-Hecht, J. Stötzeld, R. Frahmd, Phys. Chem. Chem. Phys. 11 (2009) 8779–8789.
[54] S. Tuti, F. Pepe, Catal. Lett. 122 (2008) 196–203.
[55] E. van Steen, M. Claeys, M.E. Dry, J. van de Loosdrecht, E.L. Viljoen, J.L. Visagie, J. Phys. Chem. B 109 (2005) 3575–3577.
[56] X. Lai, D.W. Goodman, J. Mol. Catal. A 162 (2000) 33–50.
[57] A.M. Saib, A. Borgna, J. van de Loosdrecht, P.J. van Berge, J.W. Geus, J.W. Niemantsverdriet, J. Catal. 239 (2006) 326–339.